CANCER

A personalized platform identifies trametinib plus zoledronate for a patient with KRAS-mutant metastatic colorectal cancer

Erdem Bangi[1]*, Celina Ang[2,3], Peter Smibert[1†], Andrew V. Uzilov[4,5], Alexander G. Teague[1], Yevgeniy Antipin[4,5], Rong Chen[4,5], Chana Hecht[1], Nelson Gruszczynski[1‡], Wesley J. Yon[1], Denis Malyshev[1], Denise Laspina[1], Isaiah Selkridge[2], Hope Rainey[2], Aye S. Moe[4,5], Chun Yee Lau[4,5], Patricia Taik[4,5], Eric Wilck[6], Aarti Bhardwaj[2], Max Sung[2,3], Sara Kim[7], Kendra Yum[7], Robert Sebra[4,5], Michael Donovan[3,8], Krzysztof Misiukiewicz[2,3], Eric E. Schadt[4,5,3], Marshall R. Posner[2,3], Ross L. Cagan[1,3§]

Colorectal cancer remains a leading source of cancer mortality worldwide. Initial response is often followed by emergent resistance that is poorly responsive to targeted therapies, reflecting currently undruggable cancer drivers such as *KRAS* and overall genomic complexity. Here, we report a novel approach to developing a personalized therapy for a patient with treatment-resistant metastatic KRAS-mutant colorectal cancer. An extensive genomic analysis of the tumor's genomic landscape identified nine key drivers. A transgenic model that altered orthologs of these nine genes in the *Drosophila* hindgut was developed; a robotics-based screen using this platform identified trametinib plus zoledronate as a candidate treatment combination. Treating the patient led to a significant response: Target and nontarget lesions displayed a strong partial response and remained stable for 11 months. By addressing a disease's genomic complexity, this personalized approach may provide an alternative treatment option for recalcitrant disease such as KRAS-mutant colorectal cancer.

INTRODUCTION

Colorectal cancer (CRC) remains the second leading cause of cancer mortality in the United States. Current standard of care includes surgery and 5-fluorouracil (5-FU)–based chemotherapy combinations such as FOLFIRI (5-FU/leucovorin/irinotecan) and FOLFOX (5-FU/leucovorin/oxaliplatin); recalcitrant or recurrent disease is then treated with one of several targeted therapies. Despite an increasing number of therapeutic options for patients with CRC, those diagnosed with metastatic disease (mCRC) have a 5-year survival rate of 11%. Furthermore, toxicities from targeted therapies are substantial: For example, many approved therapies inhibit FLT1, which is closely associated with kidney toxicity and hypertension (*1*–*3*).

Tumors with oncogenic RAS isoforms ("RAS-mutant" tumors) represent a particular challenge. An estimated 30 to 50% of CRC patient tumors include an oncogenic *KRAS* mutation; an additional ~6% of colorectal tumors contain mutations in *NRAS* or *HRAS* (*4*, *5*). Several studies, although not all, have associated RAS-mutant tumors with more aggressive metastatic disease and reduced survival (*6*–*10*). RAS-mutant CRC affects more than 60,000 patients annually, leading to more than 20,000 cancer deaths in the United States alone (*11*, *12*). More broadly, despite recent advances (*12*–*14*), therapeutic options for targeting RAS-dependent cancers remain limited (*15*–*17*).

U.S. Food and Drug Administration (FDA)–approved therapies that target the RAS pathway have shown limited efficacy in patients with KRAS-mutant mCRC. For example, the FDA-approved kinase inhibitor regorafenib (Stivarga) provides limited mCRC patient survival benefit (1.4 to 2.5 months), with substantial and highly penetrant adverse events (*3*). Other FDA-approved RAS pathway inhibitors such as trametinib (Mekinist) and immune checkpoint inhibitors have failed in CRC clinical trials for microsatellite stable disease (*18*, *19*), leading to new interest in combinations of targeted therapies (*20*, *21*). Patients with KRAS-mutant mCRC, typically presenting with right-sided tumors that are more aggressive on recurrence, are resistant to or even harmed by therapies targeting epidermal growth factor receptor (EGFR), and testing for RAS mutations are standard exclusionary criteria (*22*–*26*). Overall, patients with KRAS-mutant mCRC that develop recurrent disease have few good therapeutic options.

Our previous work demonstrated that complex RAS-mutant *Drosophila* CRC models exhibit broad aspects of transformation, including hyperproliferation, multilayering, altered apoptosis and senescence, and dissemination of transformed cells to distant sites (*27*). Here, we present the results of treating a patient with KRAS-mutant colorectal adenocarcinoma using *Drosophila* as a personalized cancer drug discovery platform (Fig. 1A). Before our treatment, the patient had shown initial partial response to chemotherapy and then tumor progression. We developed a "personalized *Drosophila* model" that altered orthologs of nine genes identified in the patient's tumor. Robotics-based high-throughput screening was then used to identify a novel combination, trametinib plus zoledronate, that improved survival of

[1]Department of Cell, Developmental and Regenerative Biology, Icahn School of Medicine at Mount Sinai, New York, NY 10029, USA. [2]Division of Hematology and Medical Oncology, Department of Medicine, Icahn School of Medicine at Mount Sinai, New York, NY 10029, USA. [3]Tisch Cancer Institute, Icahn School of Medicine at Mount Sinai, New York, NY 10029, USA. [4]Department of Genetics and Genomic Sciences and Icahn Institute for Genomics and Multiscale Biology, Icahn School of Medicine at Mount Sinai, New York, NY 10029, USA. [5]SEMA4, a Mount Sinai Venture, 333 Ludlow Street, South Tower, 3rd floor, Stamford, CT 06902, USA. [6]Department of Radiology, The Mount Sinai Hospital, New York, NY 10029, USA. [7]Department of Pharmacy, The Mount Sinai Hospital, New York, NY 10029, USA. [8]Department of Pathology, Icahn School of Medicine at Mount Sinai, New York, NY 10029, USA.
*Present address: Department of Biological Science, Florida State University, Tallahassee, FL 32306, USA.
†Present address: Technology Innovation Lab, New York Genome Center, New York, NY 10013, USA.
‡Present address: Mayo Clinic School of Medicine, Rochester, MN 55905, USA.
§Corresponding author. Email: ross.cagan@mssm.edu

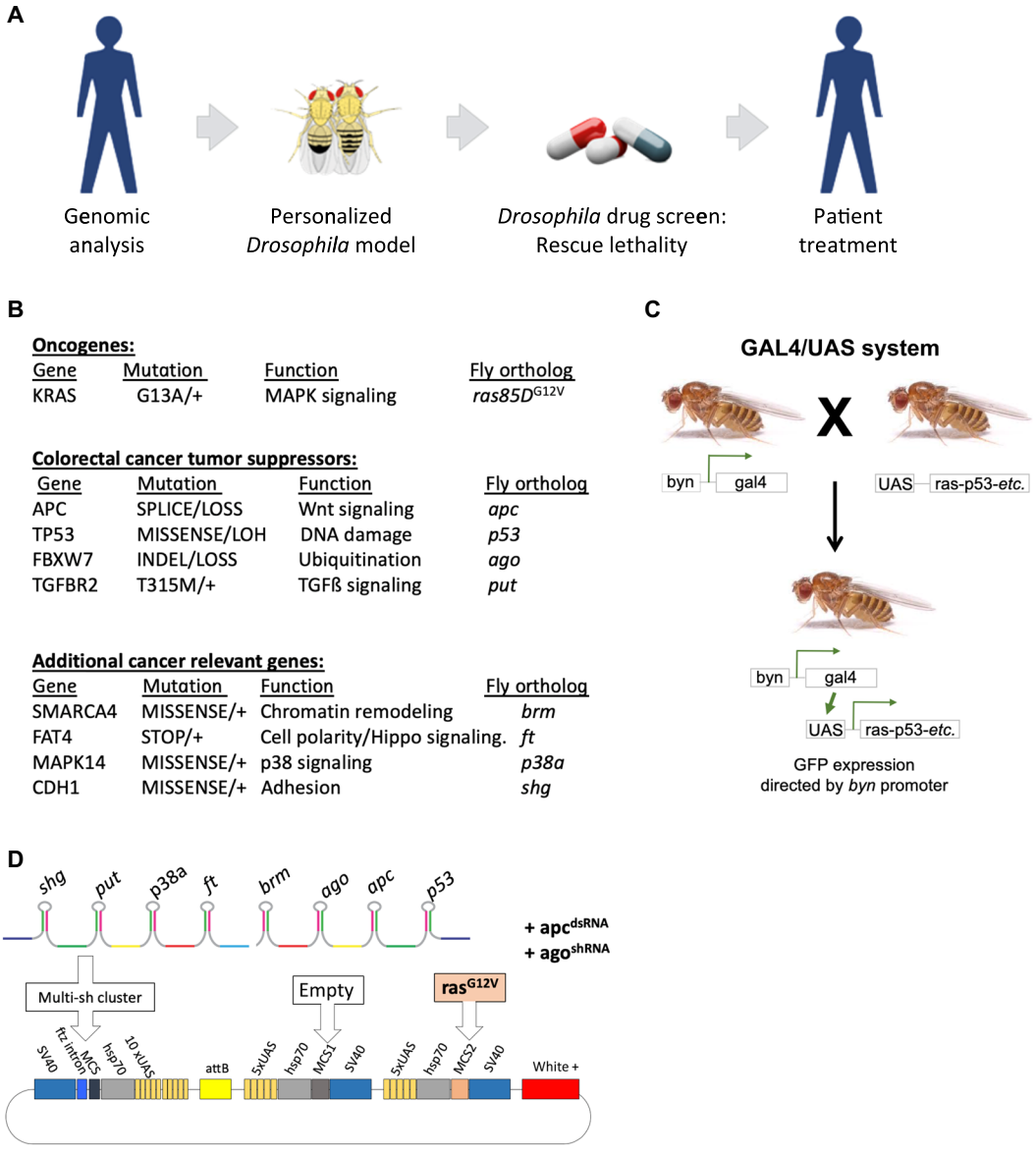

Fig. 1. Overview and construction of *Drosophila* patient model. (**A**) An outline of our approach. First, a comprehensive genomic analysis of the patient's tumor and normal DNA [copy number, whole-exome sequencing (WES), and targeted HotSpot panel] was performed. Then, a personalized *Drosophila* model that captures a portion of the patient's tumor's genomic complexity was generated by targeting each *Drosophila* ortholog specifically in the *Drosophila* hindgut. After the model was validated, a high-throughput "rescue from lethality" drug screen was performed on FDA-approved drugs as single agents and in combination. Findings were then presented to a multidisciplinary tumor board. A personalized treatment plan based on the multidisciplinary tumor board's recommendation was prepared and institutional review board–approved, followed by patient treatment. (**B**) Patient's genomic landscape: Genes altered in the patient's tumor, their functions, and *Drosophila* orthologs are indicated. LOH, copy number neutral loss of heterozygosity. MAPK, mitogen-activated protein kinase. (**C**) GAL4/UAS system used for targeted genetic manipulations in *Drosophila*. Transgenes targeting nine genes (*ras85D*^{G12V}, etc.) were cloned downstream of a GAL4-responsive UAS promoter and transgenic flies generated. Transgene expression was then induced in a tissue-specific manner by crossing transgenic flies to *byn-gal4* for hindgut epithelium and to *tubulin-gal4* for ubiquitous expression. GFP, green fluorescent protein. (**D**) Personalized construct generated for the patient, targeting nine genes. This construct expressed a GAL4-inducible (i) *UAS-ras85D*^{G12V} transgene and (ii) synthetic eight-hairpin cluster targeting the *Drosophila* orthologs of the eight tumor suppressor genes. After transgenic flies were generated, transgenic constructs *UAS-ago*^{RNAi} and *UAS-apc*^{RNAi} were genetically introduced by standard genetic crosses to increase overall *ago* and *apc* knockdown.

the personalized *Drosophila* model. Treating the patient with trametinib plus zoledronate led to a partial response: Target lesions were reduced by 45% and remained stable for several months; nontarget lesions showed a similar response. Eventually, new lesions emerged that were nonresponsive to trametinib/zoledronate therapy. Given the typically poor third-line response observed in patients with KRAS-mutant mCRC, this work suggests that personalized screening using a model organism platform merits further investigation. Our results also demonstrate that drug combinations can provide a useful therapeutic alternative to single-agent targeted therapies in KRAS-mutant mCRC.

RESULTS

Clinical synopsis and treatment history

A 53-year-old man without previous comorbidities was found to have a large partially obstructing mass of the distal sigmoid colon. A

biopsy confirmed the diagnosis of colorectal adenocarcinoma. Intraoperatively, he was noted to have synchronous liver metastases. A laparoscopic lower anterior resection was performed with creation of a sigmoid end colostomy. Surgical pathology identified a moderately differentiated pT3N2a adenocarcinoma of the rectosigmoid colon with proficient DNA mismatch repair protein expression, lymphovascular and perineural invasion, and negative margins. A targeted next-generation sequencing panel identified a *KRAS(G13A)* mutation; *BRAF*, *NRAS*, and *PIK3CA* were wild type.

Six weeks after surgery, the patient initiated systemic therapy with FOLFOX and bevacizumab. Serum carcinoembryonic antigen (CEA), which was 9.6 ng/ml on the day of surgery, decreased to 7.1 ng/ml at the start of chemotherapy. After 6 months of therapy, his CEA normalized, and a repeat computed tomography (CT) of the chest, abdomen, and pelvis showed a partial response by the liver metastases. He underwent a segment 8 hepatectomy, en bloc diaphragm resection, and colostomy reversal, followed by 3 months of postoperative FOLFOX.

On a repeat CT 1 month later, multiple new lung nodules and left superior mediastinal adenopathy were identified. Serum CEA was normal at 1.8 ng/ml. The patient resumed chemotherapy with FOLFIRI and bevacizumab for an additional 6 months. Serial imaging performed during the chemotherapy regimen initially showed a slight decrease in size of the pulmonary nodules. Subsequent imaging 3 months later showed a mixed response: slight interval progression of some pulmonary nodules and stability in others. There was also an increase in scant subcentimeter retroperitoneal lymphadenopathy and a more prominent left supraclavicular lymph node. A subsequent CT 2 months later revealed progression of lung metastases plus new left axillary, subpectoral, and mediastinal adenopathy. Previously noted retroperitoneal and pelvic adenopathy had increased. Serum CEA was 2.3 ng/ml.

Anticipating possible emergence of resistant disease, we initiated an experimental personalized treatment platform (Fig. 1A) while the patient received chemotherapy. Given the limited expected efficacy of available third-line options should FOLFIRI/bevacizumab fail (*28*–*32*), the patient elected to enroll in the experimental study 2 months after the colostomy.

Genomic analysis and mutant selection

As a first step toward developing a personalized *Drosophila* model, we carried out a comprehensive analysis of the patient's tumor genomic landscape (Fig. 1A). To this end, we extracted DNA from the primary tumor specimen and patient's blood (patient-specific normal control) and performed whole-exome sequencing (WES), targeted HotSpot panel, and copy number analysis (CNA) assays. The patient's tumor exhibited a large number of variants: 132 somatic and 965 rare germline variants.

To build a patient-specific *Drosophila* model, we focused our analysis on mutations in recurrently mutated cancer driver genes and genes that regulate cancer-relevant signaling pathways and cellular processes. In addition to confirming the oncogenic KRAS(G13A) mutation, WES analysis of the patient's tumor showed biallelic loss of the well-established CRC drivers *APC*, *TP53*, and *FBXW7* and a germline heterozygous missense mutation in *TGFBR2* (Fig. 1B). We also identified heterozygous somatic mutations in *SMARCA4*, *FAT4*, and *MAPK14* and a heterozygous germline mutation in *CDH1* (Fig. 1B). While these genes are not frequently mutated in tumors, they regulate important cancer-relevant biological processes including chromatin remodeling, cell polarity, and adhesion.

CNA identified a large number of alterations that included hundreds of genes. Using immunohistochemistry to assess gene expression levels, we focused our analysis on copy number alterations recurrently observed in colon tumors (*33*). The patient's tumor included a copy gain event in a region that encompassed receptor tyrosine kinases *FLT1* and *FLT3*. However, immunohistochemistry analysis of the tumor specimen did not reveal an increase in the levels of either protein, and they were not included in the *Drosophila* model.

Model building and validation

To build a *Drosophila* model that reflected the patient's specific genomic complexity, we altered *Drosophila* orthologs of the nine genes identified in our genomic analysis (Fig. 1B) in the fly's hindgut using the GAL4/UAS expression system (Fig. 1C) (*34*). Specifically, we cloned transgenes downstream of *UAS*, a yeast-derived promoter that is responsive specifically to the yeast GAL4 transcription factor. To target transgenes to the hindgut, we then crossed together (i) transgenic flies containing a stable genomic insertion of *UAS-transgenes* with (ii) flies directing GAL4 expression in the hindgut (*byn-GAL4*; Fig. 1C). We included a *UAS-GFP* reporter to visualize transformed tissue.

We modified a previously developed transformation vector (*35*) to contain three UAS cloning cassettes (Fig. 1D). Oncogenic *Drosophila ras85D(G12V)* was placed under the control of one UAS promoter. To simultaneously reduce activity in eight tumor suppressors, we generated synthetic clusters of sequences encoding short hairpin RNAs (shRNAs) targeting each gene; we modeled the sequences on endogenous microRNA clusters found in *Drosophila* and human genomes (see Materials and Methods and table S1). For genes biallelically inactivated in the patient—*APC*, *TP53*, and *FBXW7*—we selected hairpins predicted to provide strong knockdown; for the remaining genes with heterozygous variants, hairpins predicted to provide moderate knockdown were used. We assembled hairpin sequences into a single oligonucleotide and placed them under the control of a separate UAS promoter (see Materials and Methods and Fig. 1D). Two stable transgenic *Drosophila* lines were generated to assess different hairpin predictions: 006.1 and 006.2 each with *ras85D(G12V)* but a different set of shRNA-based hairpin oligonucleotides targeting the same eight genes. After transgenic lines were established, we also introduced additional RNA interference (RNAi) constructs for *apc* and *ago* by standard genetic crosses to ensure strong knockdown. While both models showed effective knockdown of most target genes, model 006.1 showed a more favorable knockdown profile (fig. S1). We also used hindgut lysates to analyze knockdown of Shg and P53 proteins using commercially available antibodies; these results were consistent with our quantitative polymerase chain reaction (qPCR) data (fig. S2, A and B). Expression of the transgenes in the larval hindgut with the *byn-GAL4* driver led to substantial expansion of the anterior portion of the hindgut (Fig. 2, A and B), reflecting aspects of transformation, as we previously published (*27*). We therefore selected model 006.1 for drug screening.

Drug screening

We previously demonstrated that rescue from lethality can be used as a quantitative phenotypic readout for high-throughput drug screening. Targeting transgene expression to the developing hindgut epithelium can lead to broad transformation in the epithelium and organismal lethality; this lethality can be rescued by drugs mixed with the fly's food. A drug's ability to rescue *Drosophila* cancer models to pupariation or adulthood indicates that the drug is both effective and nontoxic.

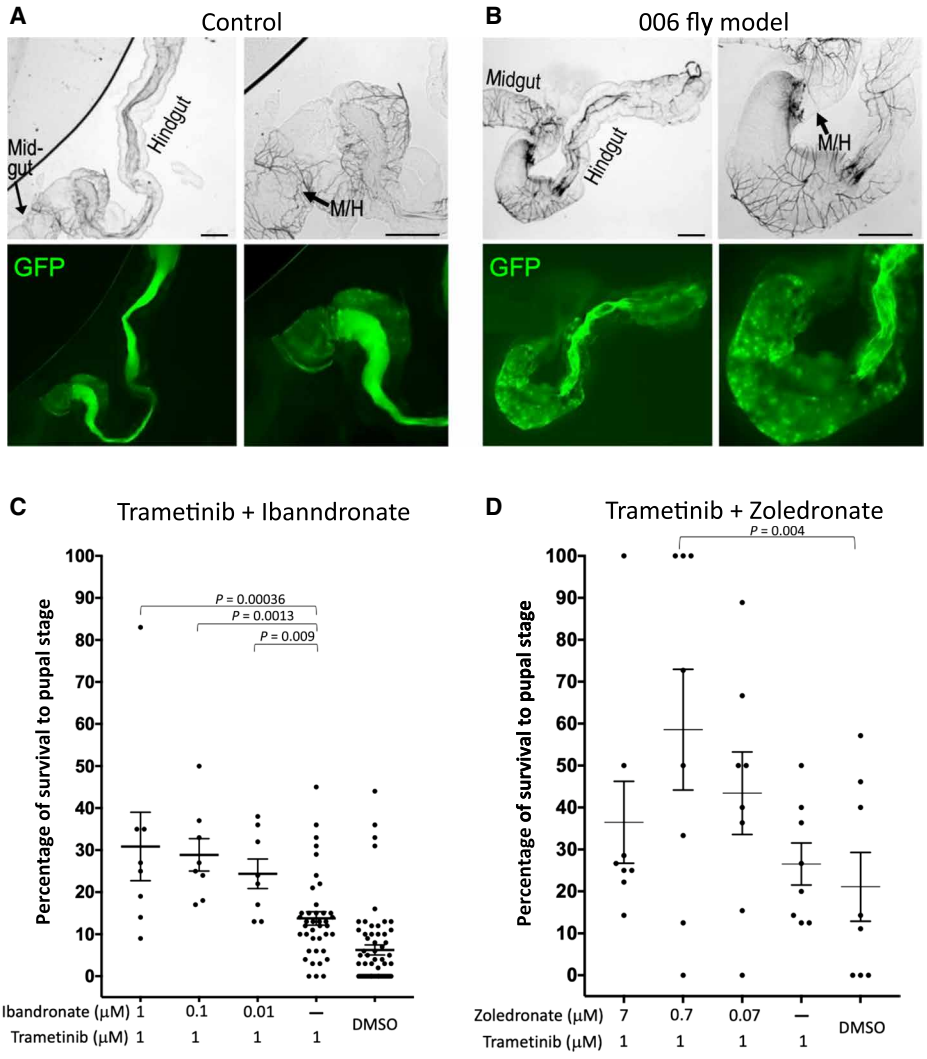

Fig. 2. Validating and screening *Drosophila* patient model. (**A**) Expressing *byn* > *GFP* in control animals highlighted the hindgut in bright-field (top panels) and expression of the *byn-GAL4* driver specific to the hindgut (bottom panels). Microscope magnifications (5× and 10×) are shown. (**B**) Expressing the 006.1 transgene set in the hindgut led to strong expansion of the anterior hindgut. The midgut/hindgut (M/H) boundaries are indicated; the dark regions in the 006 bright-field images likely reflect cell death. Image contrast was enhanced equally using Preview software for clarity. Scale bars, 100 μm. (**C** and **D**) Trametinib in combination with ibandronate or zoledronate rescued the lethality observed by the patient's personalized *Drosophila* model. Concentrations indicate final food concentrations. Each data point represents a replicate with 10 to 15 experimental and 20 to 30 control animals. Raw numbers are provided in table S2C. Error bars indicate SEM. DMSO, dimethyl sulfoxide.

For drug screening, we assembled a custom "focused FDA library" consisting of 121 drugs FDA-approved for (i) cancer, (ii) noncancer indications with reported antitumor effects, and (iii) noncancer indications with cancer-relevant targets. The first round of screening did not identify any drugs that provided significantly improved survival (see table S2A for raw data). This result is consistent with our previous work demonstrating that genetically complex cancer models are often resistant to single agents and may require drug combinations to be effective at addressing genetic complexity (*27*).

Given the presence of oncogenic *RAS* in the patient's tumor, we focused on identifying effective drug combinations that included the MEK (mitogen activated protein kinase kinase) inhibitor trametinib. Trametinib is strongly effective against oncogenic RAS alone but not against highly multigenic CRC *Drosophila* models. A combination screen focusing on noncancer drugs in a focused FDA library was screened in the presence of trametinib; the bisphosphonate class drug ibandronate was identified as strongly effective in combination with trametinib (see table S2B for raw data). These results were confirmed in an independent experiment in which trametinib was tested in combination with three different doses of ibandronate (Fig. 2C and table S2C).

Bisphosphonates have been previously reported to have antitumor effects as single agents and in combination with different tyrosine kinase inhibitors. We therefore tested two additional bisphosphonates, pamidronate and zoledronate, in combination with trametinib. Zoledronate also proved to be an effective partner for trametinib (Fig. 2D and table S2C). Ibandronate synergized with trametinib at a wider range of doses and provided a more significant rescue than zoledronate. The reason for this difference is not clear; for example, it may reflect subtle toxicity that was not apparent in controls, differences in off-target activities that lead to toxicity at higher doses, or differences in drug stability/metabolism in *Drosophila*.

A multidisciplinary tumor board that included pharmacists, oncologists, and clinical trial experts who reviewed our findings noted that oral ibandronate can cause esophagitis (*36*); intravenous administration of bisphosphonates would avoid esophagitis. Given the data supporting zoledronate as a potential anticancer agent (*37*–*40*), the tumor board recommended a combination of intravenous zoledronate and oral trametinib for the patient.

We also explored drug response at the molecular and phenotypic level in the patient model's hindgut (Fig. 3). We first evaluated RAS/MAPK signaling pathway output using dually phosphorylated extracellular signal–regulated kinase (dpERK) in hindgut lysates from drug-treated experimental animals. Lysates from the patient model demonstrated significantly increased dpERK levels compared to control animals (Fig. 3A and fig. S2C). Trametinib significantly reduced dpERK levels in the patient model, while zoledronate had no detectable effect on MAPK signaling output. Combining trametinib with zoledronate led to a stronger reduction in dpERK levels than trametinib alone, indicating that zoledronate enhances the ability of

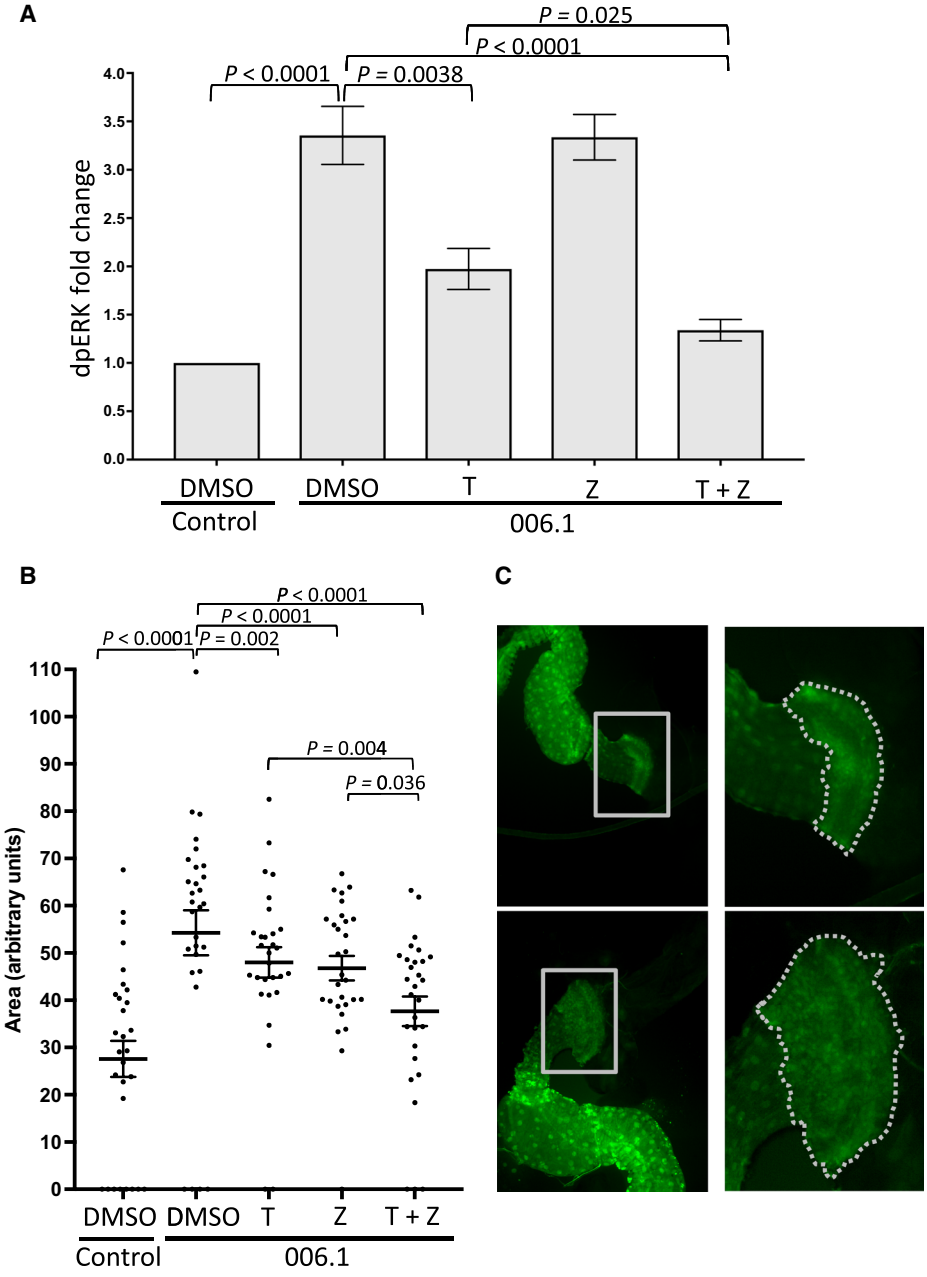

Fig. 3. Secondary assays of drug response. (**A**) Western blot analysis of MAPK signaling pathway output from control and drug-treated hindgut lysates using dpERK as a readout. Quantification represents two independent experiments with different sets of biological replicates. Each experiment was performed in triplicate with 10 hindguts per biological replicate (gel images are shown in fig. S2C). (**B** and **C**) Analysis of the expansion of the anterior hindgut in control and drug-treated animals. (B) Quantification of the anterior region of the hindgut. Data points indicate individual hindguts. (C) Two images representing the high and low ends of the size distribution observed in the assay. Quantified region of the hindgut is outlined by white dashed lines. T, 1 μM trametinib; Z, 0.7 μM zoledronate in the food. Statistical significance in (A) and (B) was determined using multiple *t* tests with Holm-Sidak correction for multiple hypotheses.

trametinib to inhibit MAPK signaling. Regarding phenotypic changes, we found a statistically significant reduction in the expansion of the anterior portion of the hindgut in the patient model in response to each single agent; the trametinib/zoledronate combination directed a stronger rescue than either drug alone (Fig. 3, B and C). Notably, the observation that zoledronate (i) partially rescued the anterior portion of the hindgut but (ii) had no effect on MAPK signaling output (Fig. 3A) suggests a complex, pleiotropic mechanism of action for the combination.

Patient treatment

Before beginning third-line therapy, the patient underwent an ophthalmologic exam and a cardiac multigated acquisition scan; both were in the normal range. A pretreatment baseline CT reported target lesions, including left axillary and para-aortic, aortocaval, and right external iliac adenopathy and a left upper lobe pulmonary nodule. The sum of the longest diameter for all target lesions was 74 mm. Pretreatment baseline CEA was 2.2 ng/ml.

Patient treatment was initiated with oral trametinib (2 mg daily) plus zoledronate (4 mg intravenously every 4 weeks). Within 2 weeks of starting therapy, the patient developed a grade 2 acneiform rash on his face, neck, and upper back, which was attributed to trametinib. The rashes progressed, and the patient was prescribed minocycline, topical clindamycin, and antihistamines. Despite these measures, the rash progressed to grade 3 in severity and the patient developed facial swelling without dyspnea or dysphonia by week 4 of therapy. Trametinib was suspended, and the patient was referred to a dermatologist, who confirmed the diagnosis of drug-induced dermatitis. His symptoms improved with the addition of prednisone. Zoledronate infusions continued every 4 weeks.

A CT of the chest, abdomen, and pelvis, performed 8 weeks from the initial start date of therapy, revealed that the sum of the target lesion diameters had decreased to 41 mm, representing a 45% decrease from baseline and partial response to treatment based on RECIST (Response Evaluation Criteria in Solid Tumors) 1.1 (Fig. 4, A and B, and table S3). The patient subsequently resumed trametinib a week later at a reduced dose of 0.5 mg every other day. Serum CEA at the time was 2.5 ng/ml. He tolerated the modified dose of trametinib well, except for grade 1 pruritis. A repeat CT scan performed 5 weeks after resuming trametinib demonstrated a sustained partial response in target lesions (sum of diameters, 41 mm). New peripancreatic and periportal adenopathy emerged, measuring 16 mm by 15 mm and 15 mm by 53 mm, respectively. On the basis of these results, the dose of trametinib was increased to 0.5 mg daily. Twelve weeks after resuming trametinib, another CT was performed, showing a 10% increase in the sum of target lesions (now 45 mm) from nadir but still 39% below baseline, indicative of a sustained partial response. The two new nontarget lesions were also slightly larger (19 mm by 16 mm and 21 mm by 65 mm), but there were no new lesions.

Given the tolerance of 0.5-mg daily trametinib without any new cutaneous toxicity, the dose was gradually increased to 1 mg daily. A further dose increase to trametinib (1.5 mg) was attempted, but the

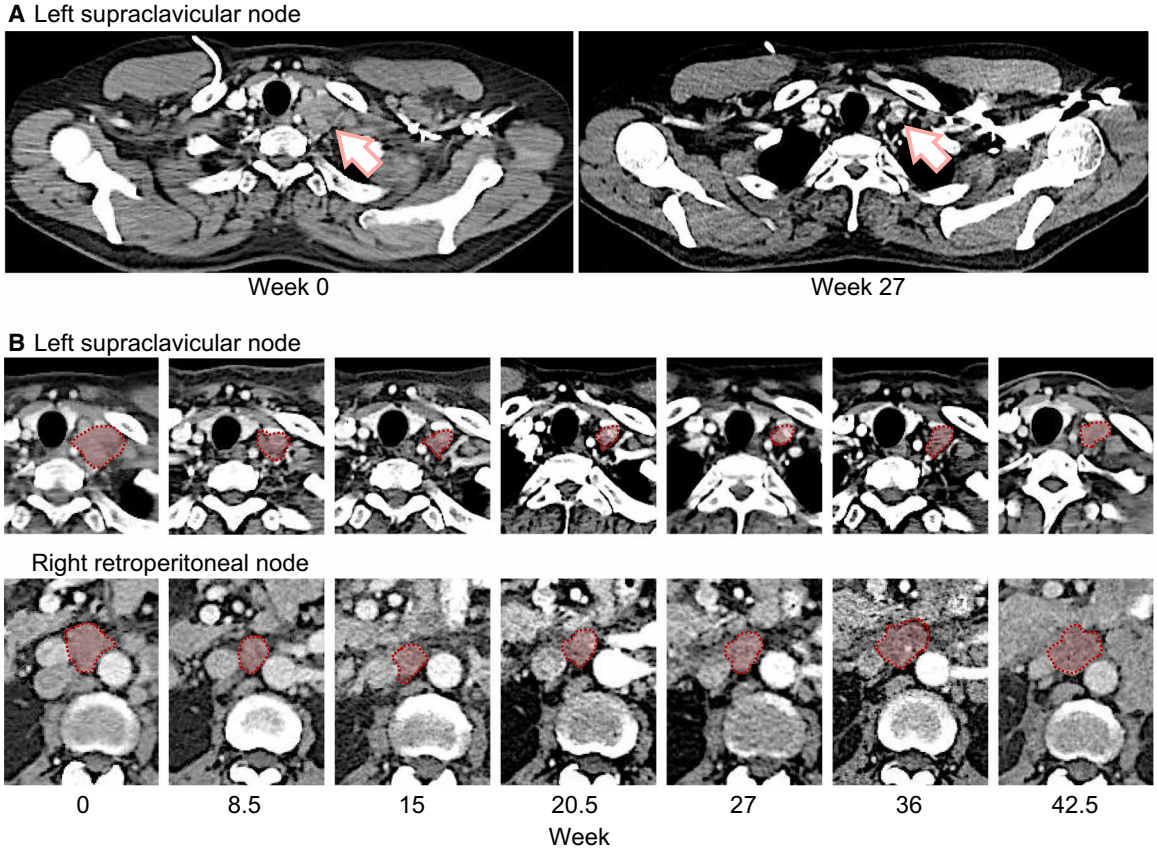

Fig. 4. Patient response. (**A**) Patient scans before treatment and 27 weeks after treatment. Arrow indicates an example of lesion in left supraclavicular node. (**B**) Two examples of target lesion shrinkage at indicated time points are highlighted by pink shading plus red dashed outline; the top panels provide detail to (A).

patient developed a pruritic rash after 1 week, causing the dose to be reduced back to 1 mg daily. A CT performed 18 weeks after resuming trametinib showed that the sum of target lesions was now 46 mm, constituting a 12% increase from nadir but still 38% lower than baseline measurements. In addition, the peripancreatic nodes had increased to 28 mm by 26 mm and the periportal nodes to 27 mm by 85 mm.

Following the CT scan, trametinib was held while a 10-day course of stereotactic radiation was initiated to the abdominal adenopathy. Trametinib was resumed 11 days later at a dose of 1 mg daily. Serum CEA was 3.0 ng/ml. At this dose of trametinib, the patient occasionally experienced mild exacerbations of the drug rash and/or skin dryness involving his face or arms, but these reactions remained grade 1 in severity. Although he still maintained a good performance status [ECOG 1 (Eastern Cooperative Oncology Group 1)], he reported increasing fatigue, occasional postprandial nausea without vomiting, and abdominal bloating. He stopped trametinib on his own for 4 days because of these symptoms and then resumed. Approximately 5 weeks after completing radiation, a new CT demonstrated that the sum of the target lesions (now 62 mm) had increased by 51% from nadir, and the total sum was now 16% below baseline. New nontarget lesions had also appeared: a left perirenal soft tissue nodule measuring 32 mm by 23 mm and an aortopulmonary window nodule measuring 15 mm by 18 mm. The irradiated periportal nodes were stable, but the peripancreatic nodes were slightly larger, measuring 28 mm by 26 mm. At this juncture, the decision was made to discontinue study therapy and switch to fourth-line therapy with regorafenib.

Overall, the patient was treated with trametinib plus zoledronate for approximately 11 months, exhibiting a maximum of 45% reduction in tumor burden. The primary toxicity was a severe rash controlled with antibiotics and antihistamines, permitting him to resume trametinib. The patient was eventually removed from treatment primarily because of emergence of previously unobserved lesions; the full genomic landscape of these lesions is unknown. We had the opportunity to explore the mutational profile of the treatment-resistant peripancreatic and periportal nodes using a specimen obtained from an endoscopic ultrasound-guided biopsy. The biopsy provided sufficient material for a targeted, high-coverage analysis using Oncomine Comprehensive Panel version 2. No new mutations were reported on the panel, ruling out most druggable targets and at least many of the mutations known to promote resistance. A similar analysis using circulating cell-free DNA identified a similar profile and also did not identify a specific resistance mechanism.

DISCUSSION

Here, we report a novel treatment approach for a patient with advanced KRAS-mutant mCRC. Before our personalized therapy, the patient had received but eventually failed multiple courses of chemotherapy. Anticipated response for this class of patients to third-line targeted therapy or chemotherapy is poor, with marginal improvement in overall survival (*41*–*43*). Instead, on the basis of extensive genomic analysis of the tumor, we developed a personalized *Drosophila* model as a whole-animal screening platform. A combination of trametinib plus a bisphosphonate reduced animal lethality. Treating the patient with trametinib/zoledronate led to a progression-free interval of 3 months overall but a partial response of target lesions lasting 8 months, including a maximum of 45% reduction in target lesions.

Our goal in creating this model was to capture tumor complexity: Drugs and lead compounds that have shown success in genetically less complex KRAS-mutant tumor models, including models that contain one to two additional targeted genes, have typically performed poorly in clinical trials. Genetically complex models can also identify candidate therapeutics that act through multiple targets, providing an opportunity for a "network approach" to address tumor complexity. Notably, regorafenib is approved as a multikinase inhibitor (*44*) that can extend survival of patients with mCRC by several weeks.

The model described here is one of the most genetically complex transgenic whole-animal disease models described to date. Still, we were able to capture only a small subset of genomic alterations observed in the patient's tumor. Using functional prediction algorithms to prioritize those variants that are most likely to deleteriously affect protein function eliminated a substantial number of variants most likely to be passenger events. We then focused on variants in genes identified as recurrently mutated drivers of cancer and those with clear cancer-relevant functions; however, our exclusion criteria are necessarily incomplete, and a large number of candidate variants remained. Further expanding the multigenic platform technology described here would provide an opportunity to generate even more sophisticated models that can better capture the genomic complexity of tumor genomic landscapes.

Most tumor genome landscapes contain a combination of heterozygous and homozygous loss of genes. Knockdown of a large number of genes to the desired level is a technically challenging issue. Use of hairpin sequences based on their predicted efficacy introduces a degree of uncertainty regarding how well they would perform in vivo, particularly in these genetically complex backgrounds. Generating two models each with a different set of hairpins targeting the same genes has been a useful approach to increasing the likelihood of success. For instance, we did not find any significant knockdown of *ft* in model 006.1 and *ft* or *shg* in model 006.2. The knockdown profiles of the models would be further optimized by replacing the ineffective hairpins with improved version. However, building and validating additional models were not feasible in the time frame of the clinical study with our current approach.

Trametinib is a potent RAS pathway inhibitor, and its clinical failure to slow progression of most KRAS-mutant solid tumor types has been unexpected. Here, we demonstrate that trametinib can act on a nine-hit *Drosophila* model when dosed in combination with a bisphosphonate; this effectiveness translated into a partial response by the patient. The nature of zoledronate's synergy with trametinib is not clear. Zoledronate has been previously demonstrated to inhibit RAS pathway signaling through direct inhibition of EGFR activity and inhibition of prenylation (*37*–*40*). In addition, zoledronate and related bisphosphonates are associated with strong protection against CRC: Women who took bisphosphonates to protect from excess bone resorption—patients with breast cancer and postmenopausal women—exhibited a 40 to 59% reduced incidence of CRC, leading to speculation of its use as a therapeutic for patients with CRC (*45*, *46*). Whether any of these activities are related to zoledronate's ability to synergize with trametinib is unclear.

Preclinical mammalian models, including patient-derived xenografts (PDXs) and organoid cultures, are key components of the drug discovery pipeline. We explored the possibility of incorporating these models into our pipeline. However, success rates for growing patient-derived tumor tissue in mice or in three-dimensional culture are generally low and highly variable, and the cost and time frame are generally prohibitive. Furthermore, these approaches require live tumor specimen from patients; our *Drosophila* pipeline on the other hand can be applied to any patient with isolated tumor tissue,

including fixed [formalin-fixed, paraffin-embedded (FFPE)] tissue. As both *Drosophila* and mammalian technologies advance, an integrated approach that combines *Drosophila* and organoid/PDX studies may prove feasible, with the latter initiated in parallel to generate sufficient models to test the most promising candidates that emerge from the *Drosophila* patient model.

In this study, we present a new, highly personalized approach to treating CRC that can be adapted for use in other tumor types and other diseases that can be modeled in *Drosophila*. The advantage of *Drosophila* is the ability to alter a large number of genes in a single tissue and screen a large number of drugs and drug combinations in a whole-animal setting with a simple readout for efficacy and toxicity. Identifying an effective, unique drug combination, trametinib plus zoledronate, emphasizes the potential for moderately high-throughput screens that can be accomplished in a time frame that is useful for treating a patient. This approach may prove especially useful in tumors with challenging profiles, for example, KRAS-mutant tumor types. Outcome data from additional patients to evaluate success rates will be necessary to determine the feasibility of integrating this approach into clinical practice.

MATERIALS AND METHODS

Enrollment

The study was regulated by three separate protocols approved by the Mount Sinai Institutional Review Board: (i) a biorepository protocol that regulated inventory and processing of tumor and patient-specific normal control (whole blood in EDTA) specimens; (ii) a molecular analysis protocol that included genomic analysis, model building/validation, and drug screening pipelines; and (iii) a treatment protocol including a personalized treatment consent for the recommended therapy after the results were reviewed and approved by a multidisciplinary tumor board.

Sample processing and genome assays

Genomic analysis was performed on (i) FFPE primary tumor specimen and (ii) whole blood collected at the time of consent to serve as a patient-matched normal control. Detailed protocols for sample processing, next-generation sequencing assays, and data integration were described previously (*47*).

Variant selection and validation

WES of tumor and blood DNA identified 132 somatic and 965 rare germline variants. We focused our analysis on genes recurrently mutated in cancers including colorectal and those involved in cancer-relevant signaling pathways and cellular processes. To determine the likelihood that observed missense variants are deleterious (e.g., negatively affect protein function), two functional prediction algorithms were used: database for functional prediction and annotation of all potential non-synonymous single nucleotide variants in the human genome (dbNSFP) and Combined Annotation Dependent Depletion (CADD) (*48*, *49*). Variants predicted to be benign (e.g., unlikely to affect protein function) by both methods were eliminated. The remaining variants were first manually reviewed by examining the raw sequence reads to exclude false positives from automated WES variant calling algorithms. In addition, each variant was independently assessed by a Pacific Biosciences sequencing platform for orthogonal validation using targeted amplicon circular consensus sequencing, as previously described (*47*, *50*). Using this method, we confirmed the presence of each variant except for *SMARCA4*, which was inconclusive strictly because of technical reasons and was included in our final selection of variants for building the *Drosophila* model.

Immunohistochemical analysis

To confirm the findings of the gene expression analysis, we performed immunohistochemical assays on 5-μm FFPE primary tumor sections for both FLT1 (1:200; catalog no. ab9540, Abcam) and FLT3 (1:100; catalog no. ab150599, Abcam) with appropriate antibody controls (*51*). Immunohistochemical scoring was performed semiquantitatively with an H-score (i.e., "histo" score) with intensity of staining ranging from 0 to 3+ multiplied by the percentage of positive expressing cells with a final score ranging from 0 to 300. The sample was considered overexpressed on the basis of a discriminating threshold greater than or equal to an H-score of 150.

Model building

Patient-specific models were generated using a multigenic UAS vector modified from a previously reported *Drosophila* transformation vector (*35*). The modified vector contains three UAS cassettes, each with their own UAS promoter, SV40 terminator sequences, and unique multiple cloning sites (MCSs). Oncogenic *Drosophila ras85D(G12V)* was PCR-amplified from a previously validated transgenic construct using primers designed to append restriction sites for enzymes Fse I and Pac I to the 5′ and 3′ ends of the product and cloned into one of the MCSs (Fig. 1D).

Short hairpins for gene knockdown were selected using DSIR, a publicly available tool for designing shRNAs (*52*) following previously established hairpin selection criteria for *Drosophila* (*35*). Individual hairpins were separated by spacer sequences found 5′ to well-expressed *Drosophila* microRNAs. To help ensure that a personalized model with a desired knockdown profile was obtained, two independent clusters that target the same eight genes using different hairpin clusters were generated (006.1 and 006.2). Hairpin, spacer, and final cluster sequences are provided in table S1.

Hairpin clusters were generated by gene synthesis (GENEWIZ). Sequence-confirmed products were then cloned into the multigenic vector using Xba I (5′) and Not I (3′). Transgenic flies were generated by PhiC31-mediated targeted integration into the *attp40* site on the second chromosome (BestGene) (*53*). To ensure strong knockdown for biallelically inactivated genes, previously validated transgenic RNAi knockdown lines for *apc* (VDRC) and *ago* (TRIP) were introduced by standard genetic crosses after transgenic flies were generated.

Model validation

Personalized models were validated by qPCR and Western blots. Experimental and control animals for validation were generated by crossing both models (006.1 and 006.2) to a *tub-gal4 tub-gal80^{ts}* line to transiently and ubiquitously induce transgene expression for 3 days. Whole larvae with the genotypes (i) *tub-gal4 tub-gal80^{ts} > UAS-006.1; UAS ago^{RNAi} UAS-apc^{RNAi}*; (ii) *tub-gal4 tub-gal80^{ts} > UAS-006.2; UAS ago^{RNAi} UAS-apc^{RNAi}*; and (iii) *tub-gal4 tub-gal80$^{ts/+}$* as controls were collected (three biological replicates per genotype and six larvae per replicate).

For protein extraction, larvae were homogenized using a motorized pestle in ice-cold 100-μl radioimmunoprecipitation assay buffer (Sigma-Aldrich) with the Phosphatase Inhibitor Cocktail Set III (EMD Millipore) and Protease Inhibitor Cocktail (Roche). Lysates were centrifuged at 4°C for 10 min at 13,000 rpm, supernatants (70 μl) were transferred to a fresh tube, and 25 μl of 4× NuPAGE LDS Sample Buffer and 10 μl of NuPAGE 10× Reducing Agent (Invitrogen) were added. After a brief spin down, samples were boiled for 10 min,

briefly spun down, and centrifuged at 4°C for 5 min at 13,000 rpm. Supernatant (80 µl) was transferred to new tubes and stored at −80°C. Western blots were performed as described previously (*27*) using the following primary and secondary antibodies: mouse anti-p53 [1:1000; Developmental Studies Hybridoma Bank (DSHB) Dmp53-H3], mouse anti-dpERK (1:1000; Sigma-Aldrich), mouse anti-syntaxin as loading control (1:1000; DSHB), and goat anti-mouse horseradish peroxidase secondary (1:10,000).

Larvae collected for RNA extraction were stored in 300-µl RNAlater (Life Technologies). RNA extraction was performed using the RNeasy Plus Kit with the RNase-free DNase Set for on-column DNA digestion (Qiagen) following the manufacturer's instructions. RNA concentration was measured using Qubit. For qPCR analysis, 1 µg of RNA was converted to complementary DNA (cDNA) using the High-Capacity RNA-to-cDNA Kit (Life Technologies), and qPCR was performed using the PerfeCTa SYBR Green FastMix for IQ (VWR Scientific). A panel of four housekeeping genes (*rpl32*, *cyp33*, *gapdh*, and *sdha*) were first assayed to identify the best candidate, and *cyp33* was selected as providing the most robust and consistent results. qPCR data were analyzed using the ΔΔC(t) method (*54*).

Model imaging

Whole guts were dissected from third instar *byn-GAL4 tubulin-GAL80^{ts} UAS-GFP/UAS-transgene* larvae that were induced at 25°C for 4 days. Control and experimental animals were fixed with 4% paraformaldehyde, washed, and mounted. Images were taken at 5× (low magnification) and 10× in Fig. 2. Quantification of the anterior portions of hindguts from drug-treated animals was performed with ImageJ software using images captured at 10× magnification.

Drug screening

Drugs in our custom focused FDA library were purchased individually as powder from the following commercial sources: Selleck Chemicals, LC Laboratories, Tocris Bioscience, and MedChemExpress. Drugs were dissolved in 100% dimethyl sulfoxide (DMSO) or water on the basis of the solubility information provided by the manufacturers. For each drug, the highest possible dose (based on solubility) that did not lead to detectable toxicity on wild-type animals was selected for screening, and drugs were aliquoted into 384-well plates.

The library was screened at a single dose for each drug along with DMSO controls (eight replicates per condition) by diluting each drug in the library 1:1000, which brings the DMSO concentration in the food to 0.1%. Drug-food mixtures were made using an automated liquid handling workstation (PerkinElmer) by adding 0.7 µl of drug into round-bottom test tubes (12 mm by 75 mm; Sarstedt), followed by 700 µl of semidefined *Drosophila* medium (recipe obtained from the Bloomington *Drosophila* Stock Center) and mixing by pipetting.

After food was solidified, a mixture of experimental and control embryos (at a ratio of 1:2 based on expected Mendelian ratios) was aliquoted into each drug/food tube (15 µl per tube). Embryo suspensions were generated using the buffer that we designed to minimize embryo clumping and settling (15% glycerol, 1% bovine serum albumin, and 0.1% Tween 20 in water). Embryos for drug screening were generated from the following cross in cages: *w/Y; UAS-006.1; UAS ago^{RNAi} UAS-apc^{RNAi}/S$_{tub\text{-}gal80}$-T* X *w UAS-dicer2; +; byn-gal4 UAS-GFP tub-gal80^{ts}/TM6, Hu, Tb*. Embryos were obtained from each cage for four to five consecutive days by providing daily a fresh apple juice plate with yeast paste. Egg lays were performed at 22°C to minimize transgene expression during embryogenesis to prevent embryonic defects or lethality that could not potentially be rescued by drug feeding. After embryos were aliquoted, drug tubes were transferred to 25°C to induce transgene expression. After 2 weeks, the number of surviving experimental pupae (EP) was counted in each tube. Drugs that showed significantly higher numbers of experimental survivors compared to vehicle controls (multiple Student's *t* tests corrected for multiple comparisons using the Holm-Sidak method, PRISM software) were considered hits.

Drug combination screens were performed by combining trametinib at its screening dose (1 µM in the food) with each drug in the library and mixing with *Drosophila* medium (eight replicates for each combination). DMSO and trametinib alone served as controls. Drug combinations identified as candidate hits were retested in an independent experiment by combining the screening dose of trametinib with three different doses of each partner drug (original screening dose and 10 and 1% of screening dose). Experimental and control pupae (EP and CP, respectively) were counted for each tube, and percentage of survival to pupal stage was calculated using the formula $[(EP \times 2/CP) \times 100]$. Statistical analysis was performed as described above.

SUPPLEMENTARY MATERIALS

Supplementary material for this article is available at http://advances.sciencemag.org/cgi/content/full/5/5/eaav6528/DC1

Fig. S1. Validation of patient's personalized *Drosophila* model (see Materials and Methods for details).

Fig. S2. Validation of patient's personalized *Drosophila* model and drug response from hindgut lysates (see Materials and Methods for details).

Table S1. Multi-hairpin cluster sequences for patient's personalized model.

Table S2. Raw drug screening and testing data.

Table S3. Patient's tumor measurements.

REFERENCES AND NOTES

1. H. Izzedine, O. Rixe, B. Billemont, A. Baumelou, G. Deray, Angiogenesis inhibitor therapies: Focus on kidney toxicity and hypertension. *Am. J. Kidney Dis.* **50**, 203–218 (2007).
2. S. R. Hayman, N. Leung, J. P. Grande, V. D. Garovic, VEGF inhibition, hypertension, and renal toxicity. *Curr. Oncol. Rep.* **14**, 285–294 (2012).
3. M. Røed Skårderud, A. Polk, K. Kjeldgaard Vistisen, F. O. Larsen, D. L. Nielsen, Efficacy and safety of regorafenib in the treatment of metastatic colorectal cancer: A systematic review. *Cancer Treat. Rev.* **62**, 61–73 (2018).
4. Y. Y. Chang, P. C. Lin, H. H. Lin, J. K. Lin, W. S. Chen, J. K. Jiang, S. H. Yang, W. Y. Liang, S. C. Chang, Mutation spectra of RAS gene family in colorectal cancer. *Am. J. Surg.* **212**, 537–544.e3 (2016).
5. E. Valtorta, S. Misale, A. Sartore-Bianchi, I. D. Nagtegaal, F. Paraf, C. Lauricella, V. Dimartino, S. Hobor, B. Jacobs, C. Ercolani, S. Lamba, E. Scala, S. Veronese, P. Laurent-Puig, S. Siena, S. Tejpar, M. Mottolese, C. J. A. Punt, M. Gambacorta, A. Bardelli, F. Di Nicolantonio, KRAS gene amplification in colorectal cancer and impact on response to EGFR-targeted therapy. *Int. J. Cancer* **133**, 1259–1265 (2013).
6. R. P. Jones, P. A. Sutton, J. P. Evans, R. Clifford, A. McAvoy, J. Lewis, A. Rousseau, R. Mountford, D. McWhirter, H. Z. Malik, Specific mutations in KRAS codon 12 are associated with worse overall survival in patients with advanced and recurrent colorectal cancer. *Br. J. Cancer* **116**, 923–929 (2017).
7. G. Karagkounis, M. S. Torbenson, H. D. Daniel, N. S. Azad, L. A. Diaz Jr., R. C. Donehower, K. Hirose, N. Ahuja, T. M. Pawlik, M. A. Choti, Incidence and prognostic impact of KRAS and BRAF mutation in patients undergoing liver surgery for colorectal metastases. *Cancer* **119**, 4137–4144 (2013).
8. H. S. Kim, J. S. Heo, J. Lee, J. Y. Lee, M.-Y. Lee, S. H. Lim, W. Y. Lee, S. H. Kim, Y. A. Park, Y. B. Cho, S. H. Yun, S. T. Kim, J. O. Park, H. Y. Lim, Y. S. Choi, W. I. Kwon, H. C. Kim, Y. S. Park, The impact of KRAS mutations on prognosis in surgically resected colorectal cancer patients with liver and lung metastases: A retrospective analysis. *BMC Cancer* **16**, 120 (2016).
9. A. L. Russo, D. R. Borger, J. Szymonifka, D. P. Ryan, J. Y. Wo, L. S. Blaszkowsky, E. L. Kwak, J. N. Allen, R. C. Wadlow, A. X. Zhu, J. E. Murphy, J. E. Faris, D. Dias-Santagata, K. M. Haigis, L. W. Ellisen, A. J. Iafrate, T. S. Hong, Mutational analysis and clinical correlation of metastatic colorectal cancer. *Cancer* **120**, 1482–1490 (2014).

10. Y. Umeda, T. Nagasaka, Y. Mori, H. Sadamori, D.-S. Sun, S. Shinoura, R. Yoshida, D. Satoh, D. Nobuoka, M. Utsumi, K. Yoshida, T. Yagi, T. Fujiwara, Poor prognosis of KRAS or BRAF mutant colorectal liver metastasis without microsatellite instability. *J. Hepatobiliary Pancreat. Sci.* **20**, 223–233 (2013).
11. H. J. N. Andreyev, A. R. Norman, D. Cunningham, J. Oates, B. R. Dix, B. J. Iacopetta, J. Young, T. Walsh, R. Ward, N. Hawkins, M. Beranek, P. Jandik, R. Benamouzig, E. Jullian, P. Laurent-Puig, S. Olschwang, O. Muller, I. Hoffmann, H. M. Rabes, C. Zietz, C. Troungos, C. Valavanis, S. T. Yuen, J. W. C. Ho, C. T. Croke, D. P. O'Donoghue, W. Giaretti, A. Rapallo, A. Russo, V. Bazan, M. Tanaka, K. Omura, T. Azuma, T. Ohkusa, T. Fujimori, Y. Ono, M. Pauly, C. Faber, R. Glaesener, A. F. P. M. . Goeij, J. W. Arends, S. N. Andersen, T. Lövig, J. Breivik, G. Gaudernack, O. P. F. Clausen, P. D. Angelis, G. I. Meling, T. O. Rognum, R. Smith, H. S. Goh, A. Font, R. Rosell, X. F. Sun, H. Zhang, J. Benhattar, L. Losi, J. Q. Lee, S. T. Wang, P. A. Clarke, S. Bell, P. Quirke, V. J. Bubb, J. Piris, N. R. Cruickshank, D. Morton, J. C. Fox, F. al-Mulla, N. Lees, C. N. Hall, D. Snary, K. Wilkinson, D. Dillon, J. Costa, V. E. Pricolo, S. D. Finkelstein, J. S. Thebo, A. J. Senagore, S. A. Halter, S. Wadler, S. Malik, K. Krtolica, N. Urosevic, Kirsten ras mutations in patients with colorectal cancer: the 'RASCAL II' study. *Br. J. Cancer* **85**, 692–696 (2001).
12. J. M. Ostrem, U. Peters, M. L. Sos, J. A. Wells, K. M. Shokat, K-Ras(G12C) inhibitors allosterically control GTP affinity and effector interactions. *Nature* **503**, 548–551 (2013).
13. S. M. Lim, K. D. Westover, S. B. Ficarro, R. A. Harrison, H. G. Choi, M. E. Pacold, M. Carrasco, J. Hunter, N. D. Kim, T. Xie, T. Sim, P. A. Jänne, M. Meyerson, J. A. Marto, J. R. Engen, N. S. Gray, Therapeutic targeting of oncogenic K-Ras by a covalent catalytic site inhibitor. *Angew. Chem. Int. Ed. Eng.* **53**, 199–204 (2014).
14. G. Zimmermann, B. Papke, S. Ismail, N. Vartak, A. Chandra, M. Hoffmann, S. A. Hahn, G. Triola, A. Wittinghofer, P. I. H. Bastiaens, H. Waldmann, Small molecule inhibition of the KRAS-PDEδ interaction impairs oncogenic KRAS signalling. *Nature* **497**, 638–642 (2013).
15. S. Misale, R. Yaeger, S. Hobor, E. Scala, M. Janakiraman, D. Liska, E. Valtorta, R. Schiavo, M. Buscarino, G. Siravegna, K. Bencardino, A. Cercek, C.-T. Chen, S. Veronese, C. Zanon, A. Sartore-Bianchi, M. Gambacorta, M. Gallicchio, E. Vakiani, V. Boscaro, E. Medico, M. Weiser, S. Siena, F. D. Nicolantonio, D. Solit, A. Bardelli, Emergence of *KRAS* mutations and acquired resistance to anti-EGFR therapy in colorectal cancer. *Nature* **486**, 532–536 (2012).
16. R. Nazarian, H. Shi, Q. Wang, X. Kong, R. C. Koya, H. Lee, Z. Chen, M.-K. Lee, N. Attar, H. Sazegar, T. Chodon, S. F. Nelson, G. McArthur, J. A. Sosman, A. Ribas, R. S. Lo, Melanomas acquire resistance to B-RAF(V600E) inhibition by RTK or N-RAS upregulation. *Nature* **468**, 973–977 (2010).
17. A. G. Stephen, D. Esposito, R. K. Bagni, F. McCormick, Dragging ras back in the ring. *Cancer Cell* **25**, 272–281 (2014).
18. G. S. Falchook, K. D. Lewis, J. R. Infante, M. S. Gordon, N. J. Vogelzang, D. J. DeMarini, P. Sun, C. Moy, S. A. Szabo, L. T. Roadcap, V. G. Peddareddigari, P. F. Lebowitz, N. T. Le, H. A. Burris III, W. A. Messersmith, P. J. O'Dwyer, K. B. Kim, K. Flaherty, J. C. Bendell, R. Gonzalez, R. Kurzrock, L. A. Fecher, Activity of the oral MEK inhibitor trametinib in patients with advanced melanoma: A phase 1 dose-escalation trial. *Lancet Oncol.* **13**, 782–789 (2012).
19. J. R. Infante, L. A. Fecher, G. S. Falchook, S. Nallapareddy, M. S. Gordon, C. Becerra, D. J. DeMarini, D. S. Cox, Y. Xu, S. R. Morris, V. G. Peddareddigari, N. T. Le, L. Hart, J. C. Bendell, G. Eckhardt, R. Kurzrock, K. Flaherty, H. A. Burris III, W. A. Messersmith, Safety, pharmacokinetic, pharmacodynamic, and efficacy data for the oral MEK inhibitor trametinib: A phase 1 dose-escalation trial. *Lancet Oncol.* **13**, 773–781 (2012).
20. M. S. Lee, T. L. Helms, N. Feng, J. Gay, Q. E. Chang, F. Tian, J. Y. Wu, C. Toniatti, T. P. Heffernan, G. Powis, L. N. Kwong, S. Kopetz, Efficacy of the combination of MEK and CDK4/6 inhibitors in vitro and in vivo in KRAS mutant colorectal cancer models. *Oncotarget* **7**, 39595–39608 (2016).
21. E. Martinelli, F. Morgillo, T. Troiani, F. Ciardiello, Cancer resistance to therapies against the EGFR-RAS-RAF pathway: The role of MEK. *Cancer Treat. Rev.* **53**, 61–69 (2017).
22. S. Benvenuti, A. Sartore-Bianchi, F. Di Nicolantonio, C. Zanon, M. Moroni, S. Veronese, S. Siena, A. Bardelli, Oncogenic activation of the RAS/RAF signaling pathway impairs the response of metastatic colorectal cancers to anti-epidermal growth factor receptor antibody therapies. *Cancer Res.* **67**, 2643–2648 (2007).
23. F. Di Nicolantonio, M. Martini, F. Molinari, A. Sartore-Bianchi, S. Arena, P. S. De Dosso, L. Mazzucchelli, M. Frattini, S. Siena, A. Bardelli, Wild-type BRAF is required for response to panitumumab or cetuximab in metastatic colorectal cancer. *J. Clin. Oncol.* **26**, 5705–5712 (2008).
24. J. Gong, M. Cho, M. Fakih, RAS and BRAF in metastatic colorectal cancer management. *J. Gastrointest. Oncol.* **7**, 687–704 (2016).
25. A. Lièvre, J.-B. Bachet, D. L. Corre, V. Boige, B. Landi, J.-F. Emile, J.-F. Côté, G. Tomasic, C. Penna, M. Ducreux, P. Rougier, F. Penault-Llorca, P. Laurent-Puig, KRAS mutation status is predictive of response to cetuximab therapy in colorectal cancer. *Cancer Res.* **66**, 3992–3995 (2006).
26. A. B. Benson III, A. P. Venook, M. M. Al-Hawary, L. Cederquist, Y.-J. Chen, K. K. Ciombor, S. Cohen, H. S. Cooper, D. Deming, P. F. Engstrom, I. Garrido-Laguna, J. L. Grem, A. Grothey, H. S. Hochster, S. Hoffe, S. Hunt, A. Kamel, N. Kirilcuk, S. Krishnamurthi, W. A. Messersmith, J. Meyerhardt, E. D. Miller, M. F. Mulcahy, J. D. Murphy, S. Nurkin, L. Saltz, S. Sharma, D. Shibata, J. M. Skibber, C. T. Sofocleous, E. M. Stoffel, E. Stotsky-Himelfarb, C. G. Willett, E. Wuthrick, K. M. Gregoryand, D. A. Freedman-Cass, NCCN Guidelines Insights: Colon Cancer, Version 2.2018. *J. Natl. Compr. Canc. Netw.* **16**, 359–369 (2018).
27. E. Bangi, C. Murgia, A. G. S. Teague, O. J. Sansom, R. L. Cagan, Functional exploration of colorectal cancer genomes using *Drosophila*. *Nat. Commun.* **7**, 13615 (2016).
28. G. Colucci, V. Gebbia, G. Paoletti, F. Giuliani, M. Caruso, N. G. Cartenì, B. Agostara, G. Pezzella, L. Manzione, N. Borsellino, A. Misino, S. Romito, E. Durini, S. Cordio, M. D. Seri, M. Lopez, E. Maiello, Phase III randomized trial of FOLFIRI versus FOLFOX4 in the treatment of advanced colorectal cancer: A multicenter study of the Gruppo Oncologico Dell'Italia Meridionale. *J. Clin. Oncol.* **23**, 4866–4875 (2005).
29. T. Deng, L. Zhang, X.-j. Liu, J.-m. Xu, Y.-x. Bai, Y. Wang, Y. Han, Y.-h. Li, Y. Ba, Bevacizumab plus irinotecan, 5-fluorouracil, and leucovorin (FOLFIRI) as the second-line therapy for patients with metastatic colorectal cancer, a multicenter study. *Med. Oncol.* **30**, 752 (2013).
30. B. J. Giantonio, P. J. Catalano, N. J. Meropol, P. J. O'Dwyer, E. P. Mitchell, S. R. Alberts, M. A. Schwartz, A. B. Benson III; Eastern Cooperative Oncology Group Study E3200, Bevacizumab in combination with oxaliplatin, fluorouracil, and leucovorin (FOLFOX4) for previously treated metastatic colorectal cancer: Results from the Eastern Cooperative Oncology Group Study E3200. *J. Clin. Oncol.* **25**, 1539–1544 (2007).
31. C.-Y. Qu, Y. Zheng, M. Zhou, Y. Zhang, F. Shen, J. Cao, L.-M. Xu, Value of bevacizumab in treatment of colorectal cancer: A meta-analysis. *World J. Gastroenterol.* **21**, 5072–5080 (2015).
32. L. B. Saltz, S. Clarke, E. Díaz-Rubio, W. Scheithauer, A. Figer, R. Wong, S. Koski, M. Lichinitser, T. S. Yang, F. Rivera, F. Couture, F. Sirzén, J. Cassidy, Bevacizumab in combination with oxaliplatin-based chemotherapy as first-line therapy in metastatic colorectal cancer: A randomized phase III study. *J. Clin. Oncol.* **26**, 2013–2019 (2008).
33. Cancer Genome Atlas Network, Comprehensive molecular characterization of human colon and rectal cancer. *Nature* **487**, 330–337 (2012).
34. A. H. Brand, N. Perrimon, Targeted gene expression as a means of altering cell fates and generating dominant phenotypes. *Development* **118**, 401–415 (1993).
35. J.-Q. Ni, R. Zhou, B. Czech, L.-P. Liu, L. Holderbaum, D. Yang-Zhou, H.-S. Shim, R. Tao, D. Handler, P. Karpowicz, R. Binari, M. Booker, J. Brennecke, L. A. Perkins, G. J. Hannon, N. Perrimon, A genome-scale shRNA resource for transgenic RNAi in *Drosophila*. *Nat. Methods* **8**, 405–407 (2011).
36. D. R. Guay, Ibandronate: A new oral bisphosphonate for postmenopausal osteoporosis. *Consult. Pharm.* **20**, 1036–1055 (2005).
37. P. A. Konstantinopoulos, M. V. Karamouzis, A. G. Papavassiliou, Post-translational modifications and regulation of the RAS superfamily of GTPases as anticancer targets. *Nat. Rev. Drug Discov.* **6**, 541–555 (2007).
38. H. Mo, C. E. Elson, Studies of the isoprenoid-mediated inhibition of mevalonate synthesis applied to cancer chemotherapy and chemoprevention. *Exp. Biol. Med.* **229**, 567–585 (2004).
39. W. W.-L. Wong, J. Dimitroulakos, M. D. Minden, L. Z. Penn, HMG-CoA reductase inhibitors and the malignant cell: The statin family of drugs as triggers of tumor-specific apoptosis. *Leukemia* **16**, 508–519 (2002).
40. T. Yuen, A. Stachnik, J. Iqbal, M. Sgobba, Y. Gupta, P. Lu, G. Colaianni, Y. Ji, L. L. Zhu, S. M. Kim, J. Li, P. Liu, S. Izadmehr, J. Sangodkar, J. Bailey, Y. Latif, S. Mujtaba, S. Epstein, T. F. Davies, Z. Bian, A. Zallone, A. K. Aggarwal, S. Haider, M. I. New, L. Sun, G. Narla, M. Zaidi, Bisphosphonates inactivate human EGFRs to exert antitumor actions. *Proc. Natl. Acad. Sci. U.S.A.* **111**, 17989–17994 (2014).
41. A. Grothey, E. Van Cutsem, A. Sobrero, S. Siena, A. Falcone, M. Ychou, Y. Humblet, O. Bouché, L. Mineur, C. Barone, A. Adenis, J. Tabernero, T. Yoshino, H. J. Lenz, R. M. Goldberg, D. J. Sargent, F. Cihon, L. Cupit, A. Wagner, D. Laurent; CORRECT Study Group, Regorafenib monotherapy for previously treated metastatic colorectal cancer (CORRECT): An international, multicentre, randomised, placebo-controlled, phase 3 trial. *Lancet* **381**, 303–312 (2013).
42. J. Li, S. Qin, R. Xu, T. C. Yau, B. Ma, H. Pan, J. Xu, Y. Bai, Y. Chi, L. Wang, K. H. Yeh, F. Bi, Y. Cheng, A. T. Le, J. K. Lin, T. Liu, D. Ma, C. Kappeler, J. Kalmus, T. W. Kim; CONCUR Investigators, Regorafenib plus best supportive care versus placebo plus best supportive care in Asian patients with previously treated metastatic colorectal cancer (CONCUR): A randomised, double-blind, placebo-controlled, phase 3 trial. *Lancet Oncol.* **16**, 619–629 (2015).
43. R. J. Mayer, E. Van Cutsem, A. Falcone, T. Yoshino, R. Garcia-Carbonero, N. Mizunuma, K. Yamazaki, Y. Shimada, J. Tabernero, Y. Komatsu, A. Sobrero, E. Boucher, M. Peeters, B. Tran, H. J. Lenz, A. Zaniboni, H. Hochster, J. M. Cleary, H. Prenen, F. Benedetti, H. Mizuguchi, L. Makris, M. Ito, A. Ohtsu; RECOURSE Study Group, Randomized trial of TAS-102 for refractory metastatic colorectal cancer. *N. Engl. J. Med.* **372**, 1909–1919 (2015).
44. S. M. Wilhelm, J. Dumas, L. Adnane, M. Lynch, C. A. Carter, G. Schütz, K.-H. Thierauch, D. Zopf, Regorafenib (BAY 73-4506): A new oral multikinase inhibitor of angiogenic, stromal and oncogenic receptor tyrosine kinases with potent preclinical antitumor activity. *Int. J. Cancer* **129**, 245–255 (2011).

45. M. Pazianas, B. Abrahamsen, P. A. Eiken, R. Eastell, R. G. Russell, Reduced colon cancer incidence and mortality in postmenopausal women treated with an oral bisphosphonate—Danish National Register Based Cohort Study. *Osteoporos. Int.* **23**, 2693–2701 (2012).
46. G. Rennert, M. Pinchev, H. S. Rennert, S. B. Gruber, Use of bisphosphonates and reduced risk of colorectal cancer. *J. Clin. Oncol.* **29**, 1146–1150 (2011).
47. A. V. Uzilov, W. Ding, M. Y. Fink, Y. Antipin, A. S. Brohl, C. Davis, C. Y. Lau, C. Pandya, H. Shah, Y. Kasai, J. Powell, M. Micchelli, R. Castellanos, Z. Zhang, M. Linderman, Y. Kinoshita, M. Zweig, K. Raustad, K. Cheung, D. Castillo, M. Wooten, I. Bourzgui, L. C. Newman, G. Deikus, B. Mathew, J. Zhu, B. S. Glicksberg, A. S. Moe, J. Liao, L. Edelmann, J. T. Dudley, R. G. Maki, A. Kasarskis, R. F. Holcombe, M. Mahajan, K. Hao, B. Reva, J. Longtine, D. Starcevic, R. Sebra, M. J. Donovan, S. Li, E. E. Schadt, R. Chen, Development and clinical application of an integrative genomic approach to personalized cancer therapy. *Genome Med.* **8**, 62 (2016).
48. M. Kircher, D. M. Witten, P. Jain, B. J. O'Roak, G. M. Cooper, J. Shendure, A general framework for estimating the relative pathogenicity of human genetic variants. *Nat. Genet.* **46**, 310–315 (2014).
49. X. Liu, C. Wu, C. Li, E. Boerwinkle, dbNSFP v3.0: A one-stop database of functional predictions and annotations for human nonsynonymous and splice-site SNVs. *Hum. Mutat.* **37**, 235–241 (2016).
50. A. V. Uzilov, K. C. Cheesman, M. Y. Fink, L. C. Newman, C. Pandya, Y. Lalazar, M. Hefti, M. Fowkes, G. Deikus, C. Y. Lau, A. S. Moe, Y. Kinoshita, Y. Kasai, M. Zweig, A. Gupta, D. Starcevic, M. Mahajan, E. E. Schadt, K. D. Post, M. J. Donovan, R. Sebra, R. Chen, E. B. Geer, Identification of a novel *RASD1* somatic mutation in a *USP8*-mutated corticotroph adenoma. *Cold Spring Harb. Mol. Case Stud.* **3**, a001602 (2017).
51. M. J. Donovan, A. Kotsianti, V. Bayer-Zubek, D. Verbel, M. Teverovskiy, C. Cordon-Cardo, J. Costa, F. A. Greco, J. D. Hainsworth, D. V. Parums, A systems pathology model for predicting overall survival in patients with refractory, advanced non-small-cell lung cancer treated with gefitinib. *Eur. J. Cancer* **45**, 1518–1526 (2009).
52. J.-P. Vert, N. Foveau, C. Lajaunie, Y. Vandenbrouck, An accurate and interpretable model for siRNA efficacy prediction. *BMC Bioinformatics* **7**, 520 (2006).
53. J. Bischof, R. K. Maeda, M. Hediger, F. Karch, K. Basler, An optimized transgenesis system for *Drosophila* using germ-line-specific φC31 integrases. *Proc. Natl. Acad. Sci. U.S.A.* **104**, 3312–3317 (2007).
54. R. Sopko, M. Foos, A. Vinayagam, B. Zhai, R. Binari, Y. Hu, S. Randklev, L. A. Perkins, S. P. Gygi, N. Perrimon, Combining genetic perturbations and proteomics to examine kinase-phosphatase networks in *Drosophila* embryos. *Dev. Cell* **31**, 114–127 (2014).

Acknowledgments: We acknowledge the Cagan Laboratory for important discussions during the progression of the study and the Genomics Core Facility at the Icahn Institute and Department of Genetics and Genomic Sciences for technical support. Computational resources and staff expertise were provided by the Department of Scientific Computing at the Icahn School of Medicine at Mount Sinai. We acknowledge support from the Novartis Patient Assistance Program. A patent application has been filed related to this work. **Funding:** This work was supported by funds from the Dean's Office and by U54OD020353 from the NIH. **Author contributions**: E.B., P.S., C.H., N.G., W.J.Y., D.M., D.L., and R.L.C. were responsible for developing and screening the *Drosophila* models. E.B., A.V.U., A.G.T., Y.A., R.C., C.Y.L., R.S., E.W., M.D., E.E.S., and R.L.C. were responsible for the genomics and tissue analyses. C.A., I.S., H.R., A.S.M., P.T., A.B., M.S., S.K., K.Y., K.M., and M.R.P. were responsible for patient clinical interactions. E.B., C.A., K.M., M.R.P., and R.L.C. had the primary roles in writing the manuscript. **Competing interests:** The authors declare that they have no competing interests. **Data and materials availability:** All data and accession numbers needed to evaluate the conclusions in the paper are present in the paper and/or the Supplementary Materials. Additional data related to this paper may be requested from the authors.

Submitted 7 October 2018
Accepted 12 April 2019
Published 22 May 2019
10.1126/sciadv.aav6528

Citation: E. Bangi, C. Ang, P. Smibert, A. V. Uzilov, A. G. Teague, Y. Antipin, R. Chen, C. Hecht, N. Gruszczynski, W. J. Yon, D. Malyshev, D. Laspina, I. Selkridge, H. Rainey, A. S. Moe, C. Y. Lau, P. Taik, E. Wilck, A. Bhardwaj, M. Sung, S. Kim, K. Yum, R. Sebra, M. Donovan, K. Misiukiewicz, E. E. Schadt, M. R. Posner, R. L. Cagan, A personalized platform identifies trametinib plus zoledronate for a patient with KRAS-mutant metastatic colorectal cancer. *Sci. Adv.* **5**, eaav6528 (2019).

A personalized platform identifies trametinib plus zoledronate for a patient with KRAS-mutant metastatic colorectal cancer

Erdem Bangi, Celina Ang, Peter Smibert, Andrew V. Uzilov, Alexander G. Teague, Yevgeniy Antipin, Rong Chen, Chana Hecht, Nelson Gruszczynski, Wesley J. Yon, Denis Malyshev, Denise Laspina, Isaiah Selkridge, Hope Rainey, Aye S. Moe, Chun Yee Lau, Patricia Taik, Eric Wilck, Aarti Bhardwaj, Max Sung, Sara Kim, Kendra Yum, Robert Sebra, Michael Donovan, Krzysztof Misiukiewicz, Eric E. Schadt, Marshall R. Posner and Ross L. Cagan

Sci Adv **5** (5), eaav6528.
DOI: 10.1126/sciadv.aav6528